CO_2 desorption dynamics on specified sites and surface phase transitions of Pt(110) in steady-state CO oxidation

Izabela Rzeźnicka and Md. Goula Moula
Graduate School of Environmental Earth Science, Hokkaido University, Sapporo 060-0810, Japan

Leonard Morales de la Garza
Centro de Ciencias de la Materia Condensada, Universidad Nacional Autónoma de México, Ensenada, BC, México

Yuichi Ohno and Tatsuo Matsushima[a)]
Catalysis Research Center, Hokkaido University, Sapporo 060-0811, Japan

(Received 8 May 2003; accepted 11 August 2003)

The spatial and velocity distributions of desorbing product CO_2 were studied in the steady-state CO oxidation on Pt(110) by cross-correlation time-of-flight techniques. The surface structure transformation was monitored by LEED in the course of the catalyzed reaction. In the active region, where the surface was highly reconstructed into the missing-row form, CO_2 desorption split into two directional lobes collimated along 25° from the surface normal in the plane including the [001] direction, indicating the CO_2 formation on inclined (111) terraces. The translational temperature was maximized at the collimation angle, reaching about 1900 K. On the other hand, CO_2 desorption sharply collimated along the surface normal at CO pressures where (1×2) domains disappeared. The distribution change from an inclined desorption to a normally directed one was abrupt at the CO pressure where the half-order LEED spot already disappeared. This switching point was more sensitive than LEED towards the complete transformation from (1×2) to (1×1) and was then used to construct a surface phase diagram for working reaction sites in the pressure range from 1×10^{-7} Torr to 1×10^{-4} Torr of oxygen. The turnover frequency of CO_2 formation was enhanced on (1×2) domains with increasing CO pressure. © *2003 American Institute of Physics.*
[DOI: 10.1063/1.1615473]

I. INTRODUCTION

The catalytic oxidation of carbon monoxide is one of the prototype reactions in surface chemistry that has led to new concepts in understanding surface reactions as well as contributed significantly to the development of new advanced surface probing tools.[1–5] The product desorption dynamics (the spatial and velocity distributions and the internal energy distributions of desorbing molecules) must be sensitive to the structure of the site on which they are formed when desorbing products leave the surface before accommodation, i.e., when the product molecules hold an excess of the translational energy. The relation of desorption dynamics to the site structure would provide the most direct site-identification method applicable in the course of catalyzed reactions. However, only a few reports have been published on the product desorption dynamics on individual formation sites.[6] One of the difficulties in this kind of work is the site identification itself. The angular distribution becomes useful to identify the formation sites when they are oriented in different directions.

This paper is the first presentation of extensive desorption dynamic studies of product CO_2 in steady-state CO oxidation on Pt(110). The spatial distribution of desorbing CO_2 from inclined terraces was fully analyzed, and the desorption dynamics was successfully used to survey the surface phase boundary at relatively low reactant pressures. The resultant diagram was examined by LEED observations under the same conditions. The differences in the diagram between the two methods suggest the high CO_2 production capacity of the (1×2) domain. A surface phase diagram was also constructed at higher pressures, and the desorption dynamics was shown to be different in each region.

A clean Pt(110) surface is reconstructed into a (1×2) missing-row structure above 275 K, and the lifting of the reconstruction into the (1×1) starts at around 0.2 ML of CO(a) and is completed at 0.5 ML.[7] These two structures yield differently oriented oxygen adsorption sites, emitting product CO_2 into different directions. The (1×2) reconstructed surface consists of three-atom-wide (111) terraces declining about 30° into the [001] direction.[8] Desorbing product CO_2 from this surface showed a well-split two-directional desorption collimated at 25° off the surface normal into the [001] direction.[9] This is because desorbing product CO_2 has a high excess of translational energy and holds the orientation of the site for CO_2 formation.[4] On the other hand, CO_2 from (1×1) domains is desorbed along the surface normal. Such desorption phenomena were first observed under temperature-programmed reaction conditions.[10]

The Pt(110) surface shows peculiar structural changes in the course of catalyzed CO oxidation near the critical CO pressure where the rate-determining step switches from CO

[a)]Author to whom correspondence should be addressed. Fax: +81-11-706-3695. Electronic mail: tatmatsu@cat.hokudai.ac.jp

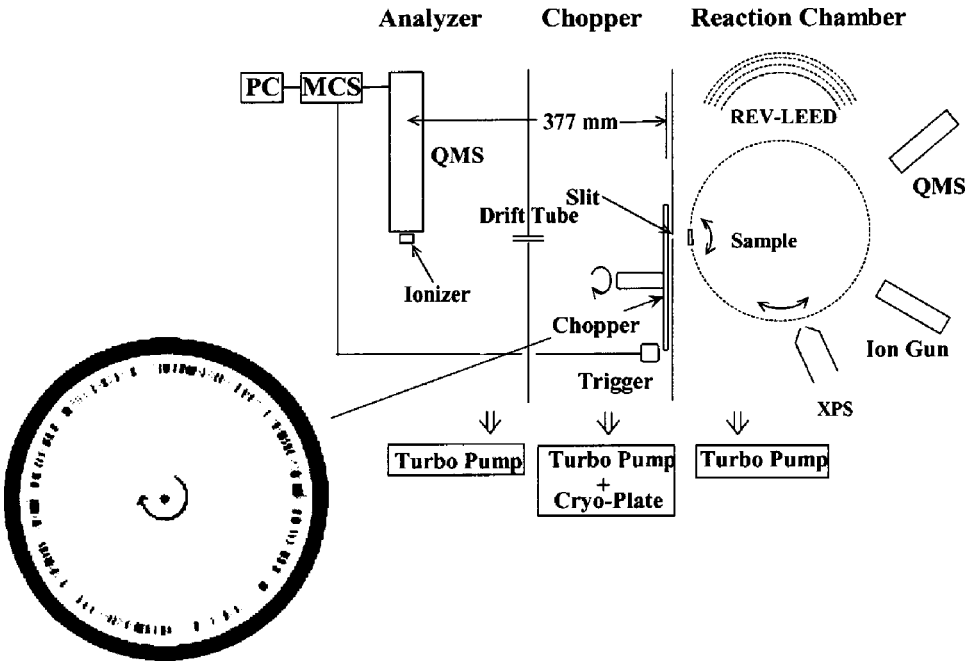

FIG. 1. Apparatus for angle-resolved product desorption combined with cross-correlation time-of-flight techniques. The insert shows the shape of the chopper blade. REV-LEED (reverse-view low-energy electron diffraction optics); QMS (quadrupole mass spectrometer); XPS (X-ray photo-electron spectroscopy optics); MCS (multi-channel scalar); trigger (photo-cell and light-emitting diode); PC (personal computer). The chopper house is pumped at 7000 l/s.

adsorption to O_2 dissociation, i.e., the surface species change from CO(a)<O(a) to CO(a)>O(a). Especially, when the critical pressure is high enough to be close to the oscillation conditions, CO(a) and O(a) form separate domains with peculiar patterns,[11,12] and those domains move on the surface, as observed in PEEM images. CO(a) domains stabilize the (1×1) form, and O(a) domains are on the (1×2) form.[11] Surface metal atoms change their positions as well as the fast movements of the reactants. Nevertheless, recent angle-resolved desorption measurements show well-split CO_2 desorption under steady-state reaction conditions,[13] indicating that the declining terraces are uniformly oriented, i.e., each (1×2) domain is not rotated against the bulk surface plane. This means that product desorption dynamics can provide surface structure information even in the course of a catalyzed reaction.

II. EXPERIMENT

The apparatus consists of a reaction chamber, a chopper house, and an analyzer (Fig. 1). The first chamber has reverse-view low-energy electron diffraction (RV-LEED), x-ray photoelectron spectroscopy optics (XPS), an Ar^+ gun, a quadruple mass spectrometer (QMS) for angle-integrated (AI) measurements, and variable leak valves for backfilling the reactant gases. It was evacuated by a turbo molecular pump with a pumping rate of 1500 l/s. The chopper house was pumped out with a turbo molecular pump and a cryo-panel cooled below 40 K (with a pumping rate of 6500 l/s). These high pumping rates can satisfactorily yield angle-resolved measurements.[14] The chopper disk has slots of equal width (1 mm×6 mm) ordered in a pseudo-random sequence (with a double sequence of 255 elements each). A time resolution of 20 μs was obtained at a chopper rotation rate of 98.04 Hz. The trigger position was determined from a curve fitting of an effusive Ar beam at room temperature to a Maxwellian distribution. The arrival time at the ionizer of another mass spectrometer in the analyzer chamber was registered on a multi-channel scalar running synchronously with the chopper blade. Time-of-flight (TOF) distributions were obtained after deconvoluting row-TOF spectra by using a standard cross-correlation deconvolution technique.[15] The flight path between the chopper blade and the ionizer measured 377 mm. The chopper house has a 1.5 mm-wide slit towards the reaction chamber. The analyzer chamber has a drift tube (50 mm in length and with a 4 mm inside diameter) toward the chopper house and another QMS for angle-resolved (AR) measurements.

A platinum crystal with a (110) plane (Crystal Preparation Laboratory, Netherlands) in a disk shape (1 mm thick and with a 10 mm diameter) was mounted on the top of rotatable manipulator. The crystal was rotated to change the desorption angle (polar angle; θ) in the normally directed plane at various crystal azimuths between [001] and [110] directions. The crystal azimuth (ϕ) is defined on the (110) plane as the angle shifted from the [001] direction, i.e., $\phi=0°$ at the [001] direction (Fig. 2). The LEED pattern showed a sharp (1×2) pattern after the surface was cleaned with standard procedures consisting of Ar^+ ion bombardments in the temperature range between 500 and 900 K and heating in 5×10^{-8} Torr oxygen at 850 K. The partial pressures of $^{12}C^{16}O$ (or $^{13}C^{16}O$ at lower pressures) (P_{CO}) and $^{16}O_2$ (P_{O2}) were kept constant by dosing gases continuously. Hereafter, ^{13}C is simply designated as C in the text. During LEED measurements, these pressures were monitored with a differentially pumped QMS in order to shield the LEED optics from the QMS filament light. The QMS sensitivity was calibrated in each experiment by referring to a Bayard–Alpert gauge. LEED patterns were recorded at the accelerating voltage of 78 eV and the long integration time of 5 seconds because of the reduced filament current to the level of nonvisible spots. Such measurements were performed after steady-state reaction conditions were established.

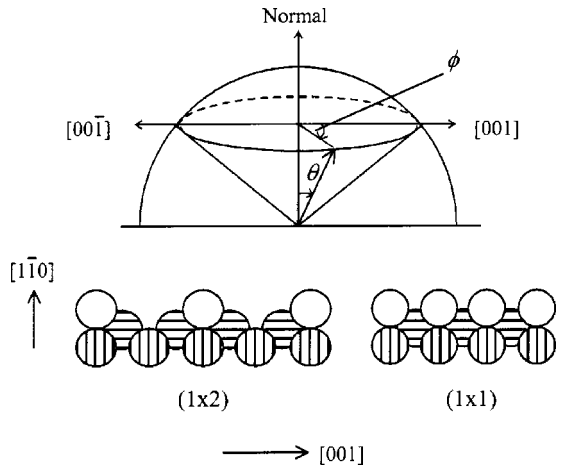

FIG. 2. Definition of the crystal azimuth (ϕ) and desorption angle (θ), and side-view of Pt(110)(1×1) and (1×2) surfaces.

III. RESULTS

A. Reaction rate

The rate of CO_2 formation under steady-state conditions was mostly monitored in the AR form. It was determined by QMS in the analyzer chamber as the difference (ΔCO_2) between the signal at the desired angle and that when the crystal was away from the line-of-sight position. In Fig. 3(a), the AR-signals at $\theta=25°$ and $\phi=0°$ are plotted against T_S, since they showed higher values than those in the normal direction in most cases except for the inhibited region above the kinetic transition. The CO_2 formation rate was negligible below 400 K and increased steeply above it, reaching a maximum between 600 and 700 K. The maximum temperature increased with increasing CO pressure. After the maximum, it decreased slowly with increasing surface temperature (T_S). Below the maximum, the signal at the higher P_{CO} runs below that at the lower P_{CO}, indicating the inhibiting effect by CO. Above the maximum, the former overcomes the other. This situation becomes clearer in the P_{CO} dependence of the CO_2 signal, as shown in Fig. 3(b). The reaction changes abruptly from a first order to a negative order at the kinetic transition point. Below this point (called the active region), the rate was insensitive to T_S. The kinetic transition point shifted to higher P_{CO} values with increasing T_S. The CO_2 signal showed a maximum at the kinetic transition and decreased with a further increase of P_{CO}. These results were obtained in both the AI- and AR-form and agree well with the general kinetic behavior of CO oxidation on platinum metals.[16]

B. Angular distribution

The angular distribution of desorbing CO_2 changes sharply around the kinetic transition. The P_{CO} dependence of both AR-signals at $\theta=25°$ and 0° (at $\phi=0°$) is shown in Fig. 4(a). In the active region, both signals increased linearly with increasing P_{CO}, i.e., no significant change was expected in the angular distribution. At the kinetic transition, both of the signals decreased sharply, but the signal at 25° was still predominant until the site-switching point, which is defined as

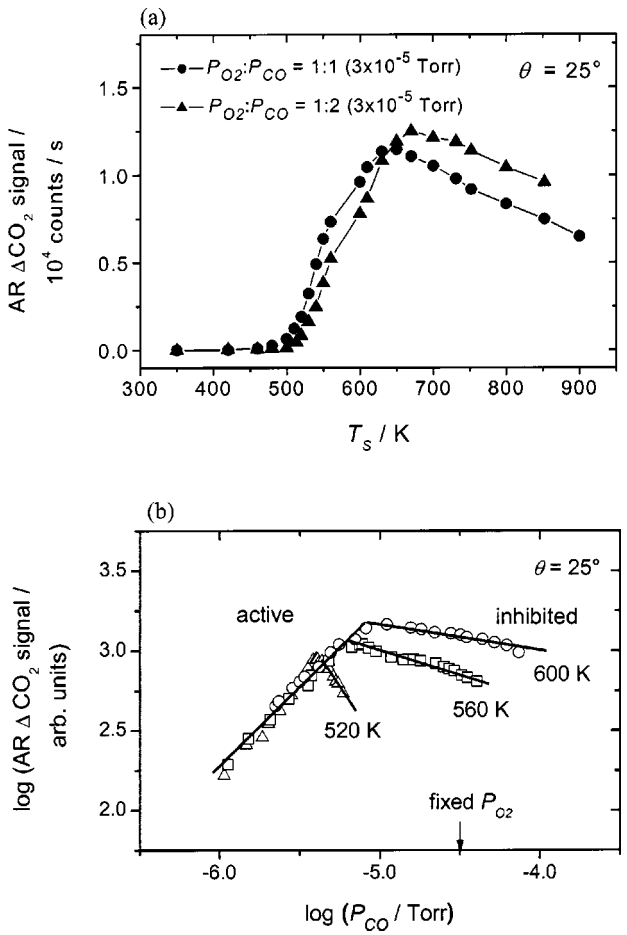

FIG. 3. (a) Steady-state CO_2 desorption signal at $\theta=25°$ as a function of T_s at different ratios of P_{O2}/P_{CO}. The total pressure is shown in the parentheses. (b) Steady-state CO_2 desorption signal at $\theta=25°$ as a function of P_{CO} at fixed $P_{O2}=3\times10^{-5}$ Torr and various T_S values.

the CO pressure where both signals become equal. Above this point, the signal at $\theta=0°$ became more intense than the other, i.e., the angular distribution changed at this point. Thus, CO_2 desorption dynamics will be separately examined in the above three regions, i.e., the active region (below the kinetic transition), the boundary region (between the kinetic transition and site-switching), and the highly inhibited region (above the site-switching).

The observed angular distributions at selected P_{CO} values in the above three regions are shown on polar coordinates in Figs. 4(b)–4(d). In the active region, two-directional desorption is clear. This distribution continued in the boundary region. It was approximated as $\cos^{11}(\theta+25)+\cos^{11}(\theta-25)$. In the highly inhibited region, the observed distribution became the normally directed form of an approximate $\cos^3\theta$ form. The sharpness of each desorption must be slightly enhanced after the sensitivity correction due to the velocity difference. As shown later, the signal at $\theta=25°$ represents mostly the inclined component from the declining (111) terrace, and that at $\theta=0°$ is mostly contributed from the normally directed component from the other parts, i.e., the (1×1) domains and boundaries between domains. Under all the conditions studied, the signal at $\theta=25°$ was mostly higher than that at $\theta=0°$ in the active region, and, above the

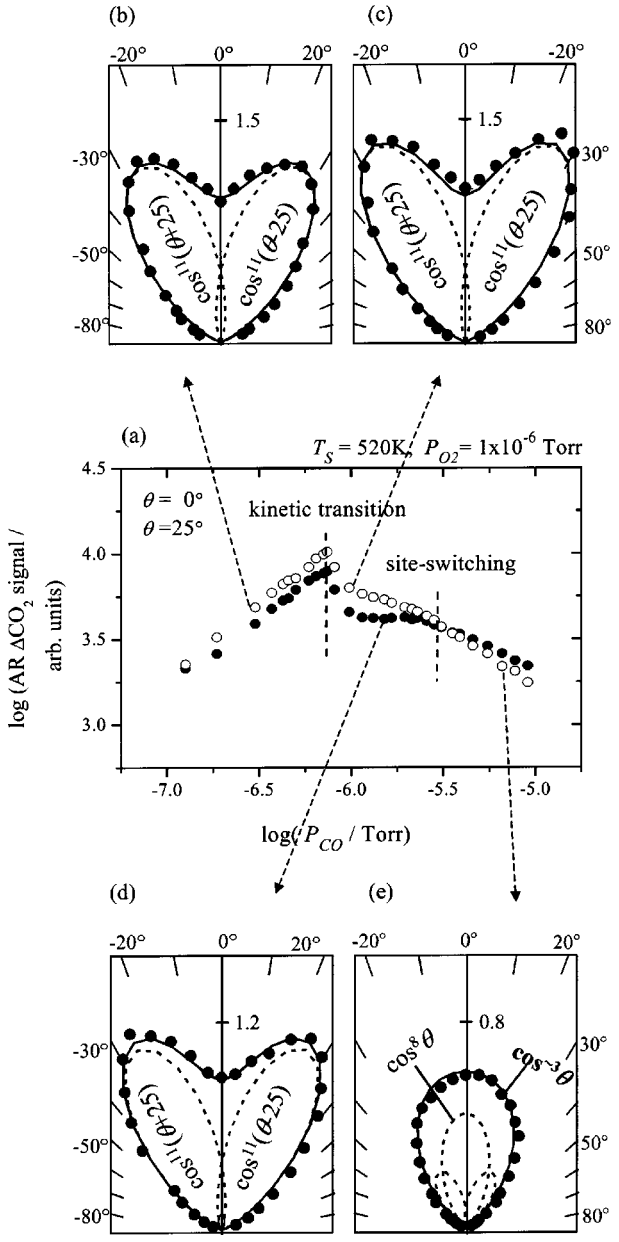

FIG. 4. (a) Steady-state angle-resolved CO_2 signals observed at $\theta=25°$ and $\theta=0°$ with CO pressures at $P_{O2}=1\times10^{-6}$ Torr and $T_S=520$ K. (b)–(e) Angular distributions of CO_2 in the plane along the [001] direction are shown in polar coordinates. The signal on the ordinate was normalized to that in the normal direction at the insert (c). The apparent distribution is indicated in bold. Typical deconvolutions are drawn by broken curves.

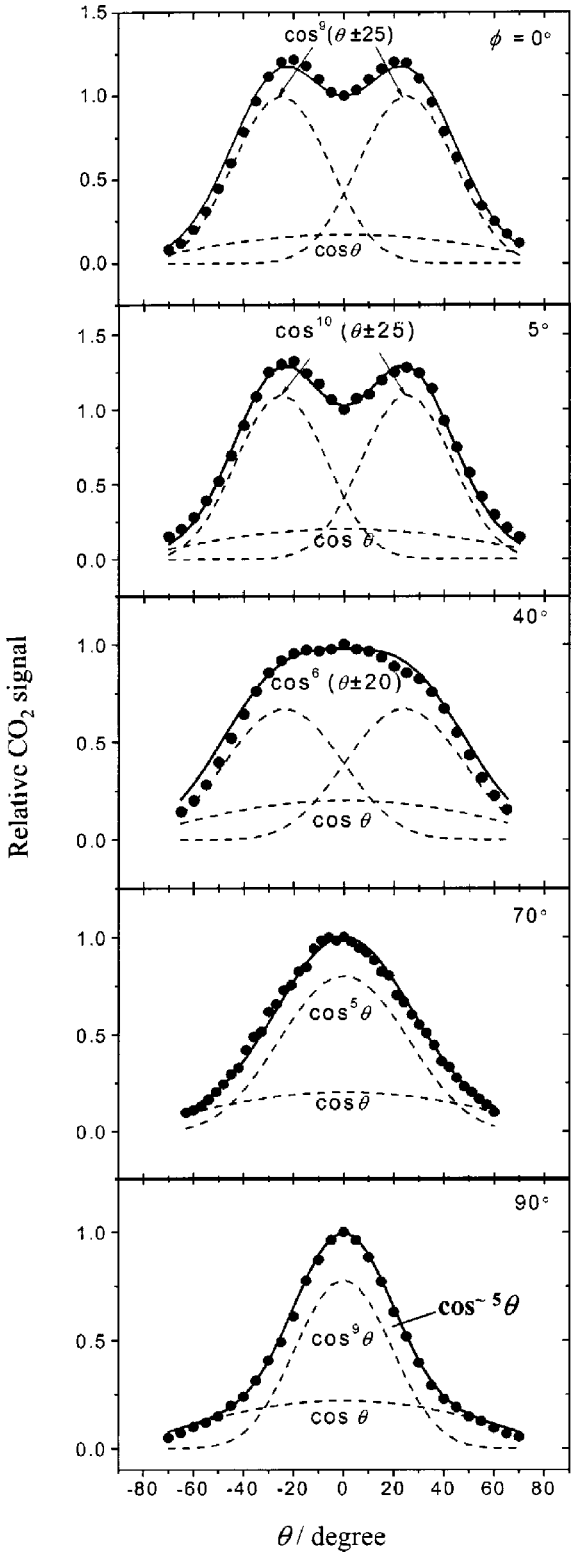

FIG. 5. Angular distributions of desorbing CO_2 at different crystal azimuths in the active region at $P_{O2}=3\times10^{-5}$ Torr and $T_s=500$ K. The signal was normalized to the value at the normal direction. Typical deconvolutions are shown by broken curves. The solid curve indicates the sum of the components. The apparent distribution is indicated in bold.

kinetic transition, especially in the boundary region, it was sensitive to both T_S and P_{CO}. This indicates that the spatial distribution of desorbing CO_2 is rather stable in both the active region and the highly inhibited region, whereas it changes drastically in the boundary region.

C. Crystal-azimuth dependence

The angular distribution of desorbing CO_2 strongly depends on the crystal azimuth. In order to characterize the desorption components, the angular distributions were examined at various crystal azimuths (Fig. 5). The characteristic distribution of CO_2 on the (1×2) reconstructed surface was observed at $\phi=0°$. At this azimuth, CO_2 desorption was split into two components collimated along $\theta=+25°$ or $-25°$ and approximated as $\cos^{9\pm2}(\theta+25)+\cos^{9\pm2}(\theta-25)$. These components approached each other with increasing ϕ value and coalesced into one component at the azimuth range of

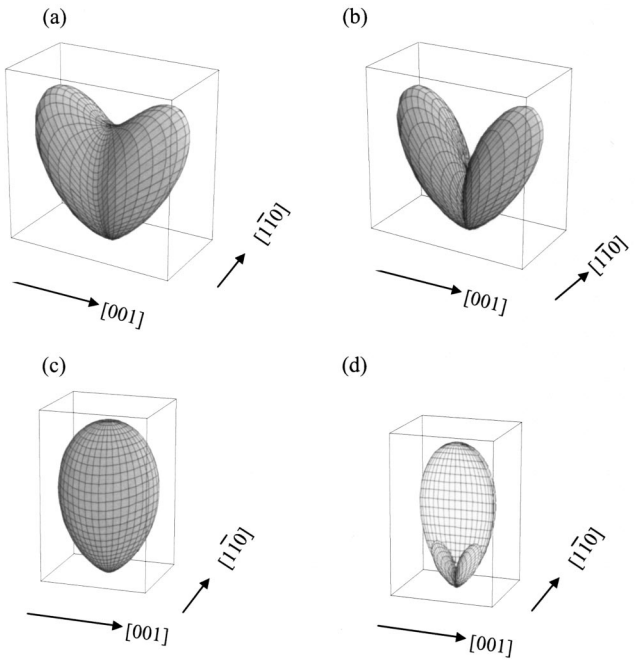

FIG. 6. Three-dimensional distribution of desorbing CO_2 in the (a) active region-experimental, (b) active region-deconvoluted, (c) highly inhibited region-experimental, and (d) highly inhibited region-deconvoluted.

$\phi=70°-90°$. The total signal over the desorption angle was maximized in the plane at $\phi=0°$ and became minimum at $\phi=90°$. The signal at $\theta=0°$ remained constant, independently of the ϕ value. This indicates that all the inclined components under the reaction conditions have been observed, i.e., there are no other inclined components. The others are more or less sharply collimated along the surface normal.

The spatial distributions of desorbing CO_2 are shown in three-dimensional polar coordinates in Fig. 6, which were drawn from the data in Fig. 5. These were drawn by assuming a symmetric distribution against the normally directed planes at $\phi=0°$ and also at $\phi=90°$. The distribution in the active region [Fig. 6(a)] was deconvoluted into two symmetric components, as shown in Fig. 6(b). In a three-dimensional way, the distribution was approximated as $\cos^{10}(\alpha\pm25)\cos^{8}(\beta)$, where α is the longitude and β is the latitude when the polar axis is taken to be parallel to the crystal azimuth [110]. In general, the relation between angles (α,β) and (θ,ϕ) is given by $\cos\theta=\cos\alpha\cos\beta$ and $\tan\phi=\tan\beta/\sin\alpha$.[17] When $\beta=0°$, the value of α becomes equal to the desorption angle in the plane along the [00$\bar{1}$] direction, and, at $\alpha=0°$, β is equal to θ along the [110] direction. The summation of the two desorption lobes can reproduce the signal at any θ and ϕ value in Fig. 5 within experimental errors. This analysis indicates that the inclined CO_2 desorption intensity can approximately be described by the sharpness of the component and the signal intensity at $\theta=25°$ and $\phi=0°$.

In the highly inhibited region (far above the kinetic transition point), the CO_2 desorption collimated along the surface normal. It was approximated as $\cos^3\theta$ at $\phi=0°$ and as $\cos^4\theta$ at $\phi=90°$. The signal is two-dimensionally described as $\cos^3\alpha\cos^4\beta$ and is drawn in polar coordinates in Fig. 6(c). However, as described in Sec. IV A, this normally directed component involved the contribution from the inclined component at $\phi=0°$. Eventually, it was deconvoluted into three components. The resultant normally directed desorption was approximated as $\cos^5\theta$ at $\phi=0°$ and as $\cos^5\theta$ at $\phi=90°$. The signal of the normally directed component is two-dimensionally described as $\cos^5\alpha\cos^5\beta$ and is drawn with the accompanied inclined desorption in polar coordinates in Fig. 6(d).

Hereafter, the angular distribution at $\phi=0°$ is mostly discussed because it is sufficient to describe the intensity of each desorption component. The intensity of each desorption component is represented by the signal at $\theta=25°$ and $\theta=0°$ in the plane along the [001] direction (at $\phi=0°$).

D. Distribution change

The angular distribution in the plane along the [001] direction did not change sharply in the active region, as explained above. It was split into two inclined components collimated at around $\pm25°$ except for the conditions at very low P_{CO} values.[13] The distribution change above the kinetic transition was sensitive to T_S and P_{O2}. The distributions at $T_s=520$ K and $P_{O2}=1\times10^{-6}$ Torr did not change around the kinetic transition, as shown in Fig. 4(a). The CO_2 signal at $\theta=25°$ was higher than that at $\theta=0°$ even above the kinetic transition point, although the total CO_2 formation was suppressed. At lower surface temperatures (typically at 480 K in Fig. 7), site-switching took place at the kinetic transition point, i.e., no boundary region was found. The two-directional desorption appeared in the active region, and, above the kinetic transition, the normally directed desorption was observed in a $\cos^3\theta$ form. At higher temperatures, the site-switching point shifted further above the kinetic transition, i.e., the boundary region became wider.[13] At higher oxygen pressures, the site-switching point moved close to the kinetic transition even at higher surface temperatures (typically at 550 K and 1×10^{-4} Torr of O_2 in Fig. 8). It should be noticed that the distribution changed in the active region at lower CO pressures.[13] A clear two-directional desorption was found close to the kinetic transition and continued even above the transition. Far above the kinetic transition, the desorption collimated along the surface normal, as approximated in a $\cos^3\theta$ form.

On the other hand, in the plane along the [1$\bar{1}$0] direction, no angular distribution changes were noticeable over the above three regions. CO_2 desorption always collimated along the surface normal in both the active and inhibited regions, as shown in Fig. 9. The observed desorption followed a $\cos^5\theta$ form in the active region and a $\cos^4\theta$ form in the inhibited region.

E. Velocity distribution

The translational energy can be used to examine the collimation position of desorption components because it is maximized at the collimation angle in the repulsive desorption.[18] It may characterize the product desorption when the product is formed on sites with different structures.

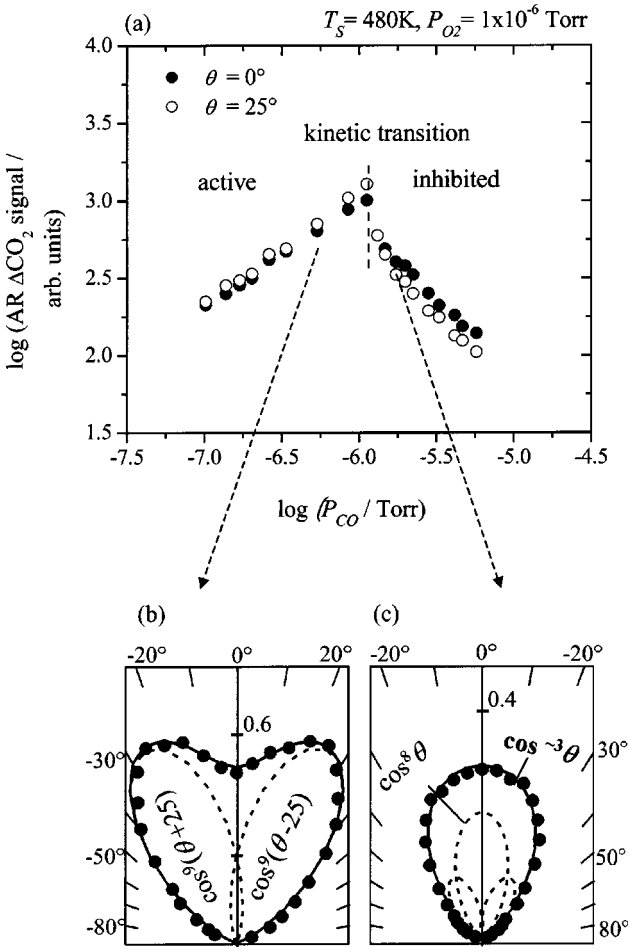

FIG. 7. (a) Steady-state angle-resolved CO_2 signals observed at $\theta=25°$ and $\theta=0°$ with CO pressures at $P_{O2}=1\times10^{-6}$ Torr and (representative low temperature) $T_S=480$ K. (b) and (c) Angular distributions of CO_2 in the plane along the [001] direction are shown in polar coordinates. The signal on the ordinate was normalized to the maximum at the kinetic transition point. The apparent distribution is indicated in bold. Typical deconvolutions are drawn by broken curves.

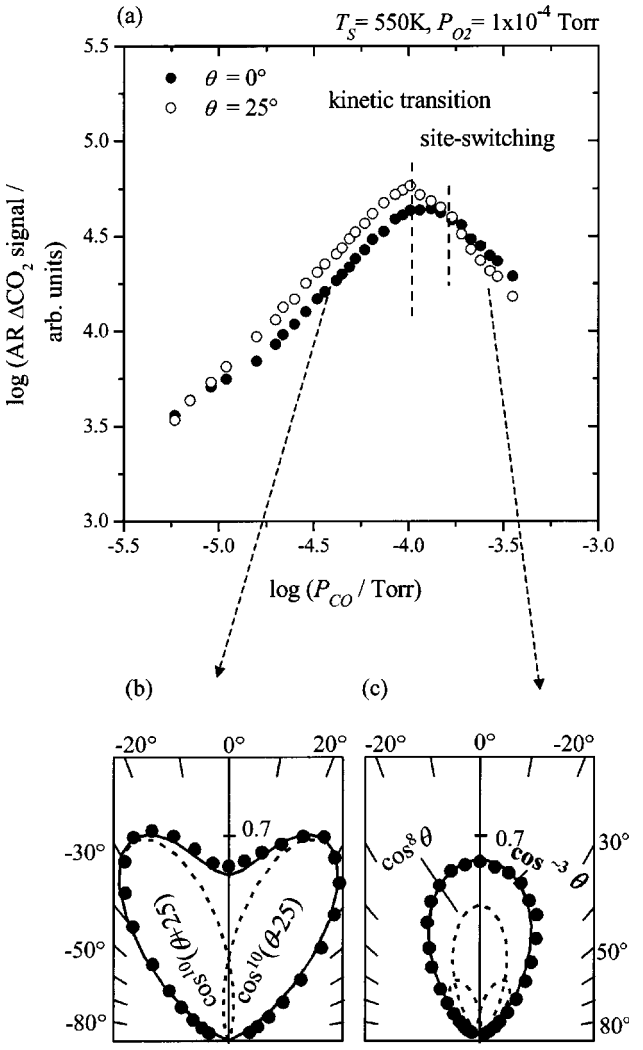

FIG. 8. (a) Steady-state angle-resolved CO_2 signals observed at $\theta=25°$ and $\theta=0°$ with CO pressures at $P_{O2}=1\times10^{-4}$ Torr and (representative high temperature) $T_S=550$ K. (b) and (c) Angular distributions of CO_2 in the plane along the [001] direction are shown in polar coordinates. The signal on the ordinate was normalized to the maximum at the kinetic transition point. The apparent distribution is indicated in bold. Typical deconvolutions are drawn by broken curves.

Velocity distributions were measured in the active region, the boundary region, and the highly inhibited region. The energy showed different values in each region.

In the active region, the translational energy of CO_2 was maximized at around $\theta=25°$, being consistent with the two-directional desorption. Typical velocity distributions at $T_S=560$ K and $P_{O2}=3\times10^{-5}$ Torr are shown in Fig. 10. Each distribution curve was approximately fitted to one modified Maxwellian form. The resultant mean energy, which is indicated in $\langle\ \rangle$, is shown in the temperature units as $T_{\langle E\rangle}=\langle E\rangle/2k$, where $\langle E\rangle$ is the mean translational energy and k is the Boltzmann constant. This average value showed a maximum at around $\theta=25°$ and decreased with a further increase in the desorption angle at $\phi=0°$, as shown in Fig. 11(a). In the active region, the value reached 1780 ± 80 K at 25° in the [001] direction and 1550 ± 40 K at the normal direction. On the other hand, the average translational energy in the [110] direction was maximized at the normal direction and reached around 1530 ± 80 K, and the energy decreased with increasing the desorption angle faster than it decreased in the [001] direction. Thus, the above maximized translational temperature at $\theta=25°$ and $\phi=0°$ and the observed two-directional desorption indicate CO_2 formation on the declining terraces of (1×2) domains in the active region.

It should be noticed that, in the velocity distributions in the plane along the [110] direction, the slow component was pronounced at an angle above 25° [Fig. 10(b)]. This indicates that desorbing CO_2 involves the thermalized component, although its amount is not significant. Therefore, we deconvoluted all the velocity distribution curves into two components, i.e., the slow and fast ones, and evaluated the translational temperature of the fast component. Here, the slow component described by a Maxwell distribution at T_S was first fitted to the observed signal, and the remaining signal after subtraction of the slow one was then fitted to a modified Maxwellian form. Typical deconvolutions are shown by broken curves in the figure. In this way, the slow component is maximized and the resultant energy of the fast component then shows the upper limit of its translation en-

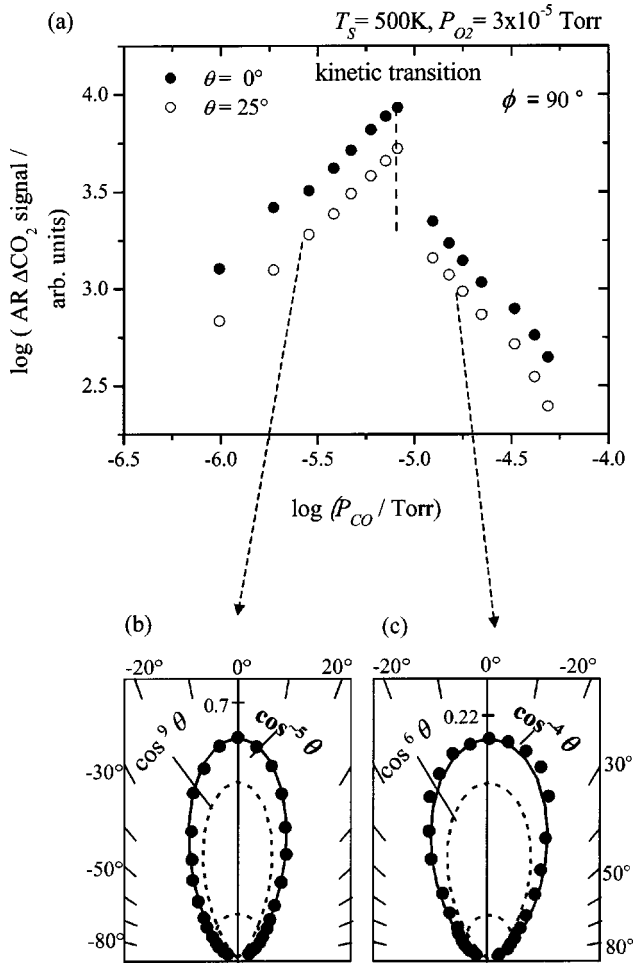

FIG. 9. (a) Steady-state angle-resolved CO_2 signals observed at $\theta=25°$ and $\theta=0°$ with CO pressures at $P_{O2}=3\times10^{-5}$ Torr and $T_S=500$ K. (b) and (c) Angular distributions of CO_2 in the plane along the [110] direction are shown in polar coordinates. The signal on the ordinate was normalized to the maximum at the kinetic transition point. The apparent distribution is indicated in bold. Typical deconvolutions are drawn by broken curves.

ergy. The resultant values are inserted in the velocity curves in the figures. The energy was plotted in Figs. 11(a)–11(c). The values after deconvolution are slightly shifted upwards compared with the data without deconvolutions.

In both the active and boundary regions, the maximum value of the fast component reached 1900±80 K at 25° along the [001] direction. The thermalized component yielded a cosine distribution and the angular distribution was then deconvoluted into a cosine form and a sharp component consisting of the remaining signal. Thus, the observed angular distributions were deconvoluted. These are also shown by broken lines in Fig. 9. The resultant normally directed component shows a $\cos^9\theta$ form along the [110] direction.

In the boundary region between the kinetic transition and the site-switching, the translational energy at $\theta=25°$ still kept the maximum value, as it did in the active region. This indicates the same desorption dynamics as that in the active region, although the signal itself was highly suppressed.

In the highly inhibited region, the average energy was maximized at the normal direction, i.e., the average value at $\theta=25°$ decreased to 1650±40 K, whereas the value at $\theta=0°$ reached 1730±80 K [Fig. 11(c)]. This observation is consistent with an enhanced normally directed desorption component observed above the site-switching. In the plane along the [110] direction, the translational energy was maximized at the normal direction, and, at higher desorption angles, the surface temperature component was highly dominated. In both [001] and [110] directions, the translational energy monotonously decreased with increasing the desorption angle.

F. LEED study

LEED observations were performed under steady-state conditions below 1×10^{-5} Torr. The results at $P_{O2}=1\times10^{-7}$ and $T_S=490$ K Torr are summarized in Fig. 12(c). The graph summarizes the spot-intensity profile at different CO pressures. The intensities of the half-order spots were significant at low pressures of CO and decreased at higher CO pressures. In the active region, a clear (1×2) LEED pattern was observed. In the inhibited region above or near the site-switching, a (1×1) pattern was found, and the half-order spots disappeared [Figs. 12(a) and 12(b)]. The half-order spot intensity, which is merely due to the (1×2) domains, is plotted against P_{CO} in Fig. 12(d). The intensity was normalized to the maximum value in the active region after the background subtraction. With increasing P_{CO}, the half-order spot intensity started to decrease already before the kinetic transition point, reaching about a half of the value at this point, and decreased further to the background level at the site-switching point. Its spot width did not change throughout the measurement, suggesting that the (1×2) domain was larger than the coherent length of the LEED optics.[19] It should be noted that the half-order spot intensity disappears faster than the signal of the two-directional CO_2 desorption.

At temperatures at which the site-switching occurs close to the kinetic transition point, i.e., no boundary region, the transformation from (1×2) to (1×1) was completed quickly at the kinetic transition point, i.e., the half-order spot intensity disappeared at the kinetic transition point.

G. Temperature dependence of the transition points

The critical CO pressure required for the kinetic transition or the site-switching was determined in a wide range of oxygen pressures and surface temperatures. At low oxygen pressure of $P_{O2}=1\times10^{-7}$ Torr, the boundary region between the kinetic transition and the site-switching was widely extended to 450 K, as shown in Fig. 13. In the figure, the logarithm of the critical CO pressure was plotted against the reciprocal of the surface temperature, so that the slope of the lines provides the activation energy for both transitions. With increasing P_{CO}, the inclined desorption was major up to the site-switching line. Above this line, the normally directed desorption became major. From the LEED data, we could confirm that the surface was in the (1×2) form below the kinetic transition line, and, above the site-switching line, in the (1×1) form. In the CO pressure range between those two lines, the surface was covered by a mixture of both forms. However, it should be noticed that the two-directional desorption was major until the site-switching line.

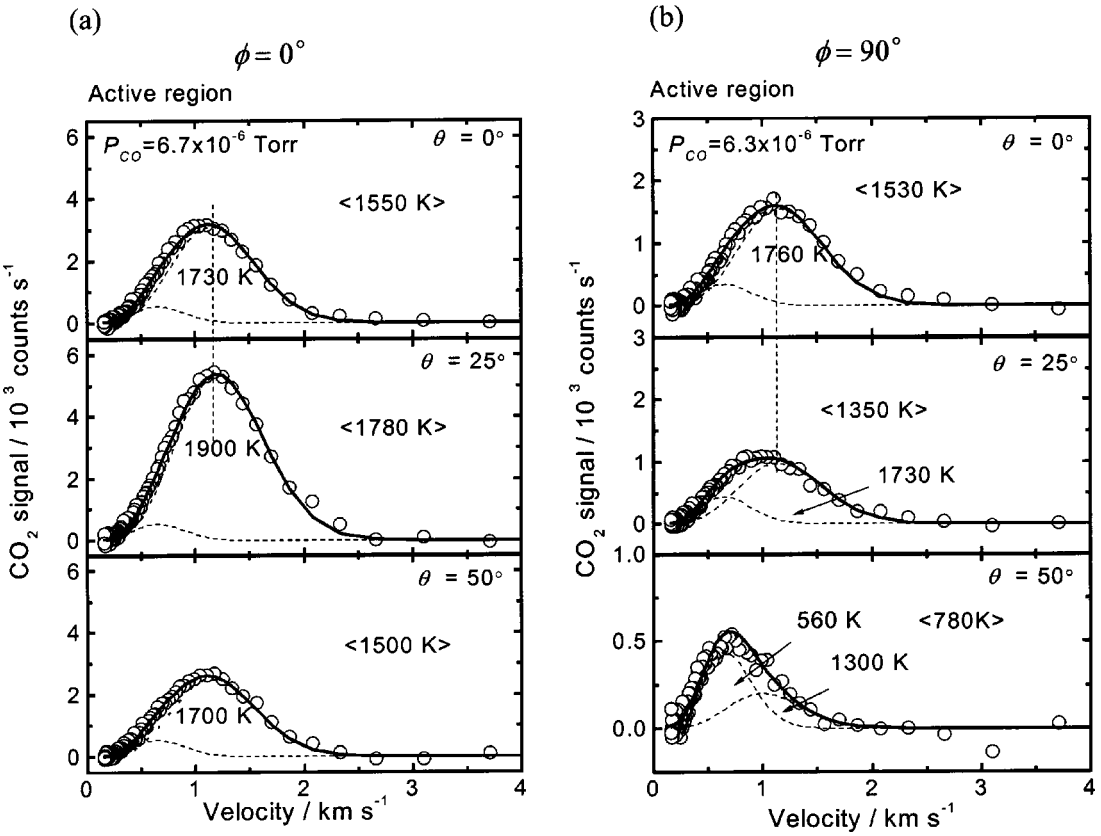

FIG. 10. Velocity distributions of desorbing CO_2 at $T_S = 560$ K and $P_{O2} = 3 \times 10^{-5}$ Torr in the active region in the plane along (a) the [001] direction and (b) the [110] direction. Typical deconvolutions into the fast and slow components are given by broken curves.

At high P_{O2}, the kinetic transition shifted to higher CO pressures, where the boundary region was limited to high temperatures, as shown in Fig. 13. At $P_{O2} = 1 \times 10^{-4}$ Torr, the site-switching line coalesced with the kinetic transition line at temperatures below 520 K, i.e., the site-switching took place at the kinetic transition point. This means that the site-switching below this temperature is merely controlled by the property of the kinetic transition. The activation energy for the kinetic transition was estimated to be 4.5 kcal/mol at $P_{O2} = 1 \times 10^{-7}$ Torr. It increased to 10 kcal/mol at $P_{O2} = 1 \times 10^{-4}$ Torr. The value for the site-switching was estimated to be 31 kcal/mol.

In general, the kinetic transition line moved to higher CO pressures with increasing the oxygen pressure, as expected from the enhanced removal of adsorbed CO. On the other hand, the site-switching line was almost independent of O_2 pressure. It was merely controlled by CO pressure and the surface temperature. This line coalesced with the kinetic transition line when P_{CO} was high enough to yield the amount of CO(a) required for the site-switching. The boundary region appeared when the CO pressure at the kinetic transition was not high enough to reach the critical amount of CO(a). Eventually, the boundary region became narrower at higher O_2 pressures.

IV. DISCUSSION

A. Deconvolution of angular distributions

The observed angular distribution in the active region changed slightly with CO pressure, as seen in Figs. 4, 7, and 8, where the signal ratio at 25° and 0° decreased at lower CO pressures. In the [001] direction, the two-directional desorption became well-split just above the kinetic transition, where the surface was covered by either CO(a) or O(a) domains. The parameters characterizing the two-directional desorption were determined by fitting a power function of the cosine of the desorption angle with the observed data, as $\cos^{11}(\theta+25)+\cos^{11}(\theta-25)$. The collimation angle of 25 degrees shifted from the normal direction of declining terraces by about 5 degrees.[13] This was already explained by the surface-smoothing effect.[20] The velocity of desorbing CO_2 is not high enough to keep the site orientation precise. Hereafter, these parameters were used to deconvolute the angular distribution curves. At P_{CO} values far below or far above the kinetic transition, the contribution from the normally directed component was enhanced, i.e., the two-directional desorption coexists with the other component.[13]

Typical deconvolutions of the angular distributions are shown by broken curves in Figs. 4(b)–4(e), 7(c), and 8(c). In this deconvolution, the contribution from the inclined desorption was maximized, i.e., the two-directional component was first fitted to the data points, and the remaining signal after its subtraction was fitted into a single power function of $\cos\theta$. The resultant component collimated along the surface normal as $\cos^8\theta$. This sharpness is consistent with the observed high velocity in the surface normal direction in the highly inhibited region. It should be noted that the sharpness of the angular distribution is quite close to that in the inclined component. The deconvolution to maximize the nor-

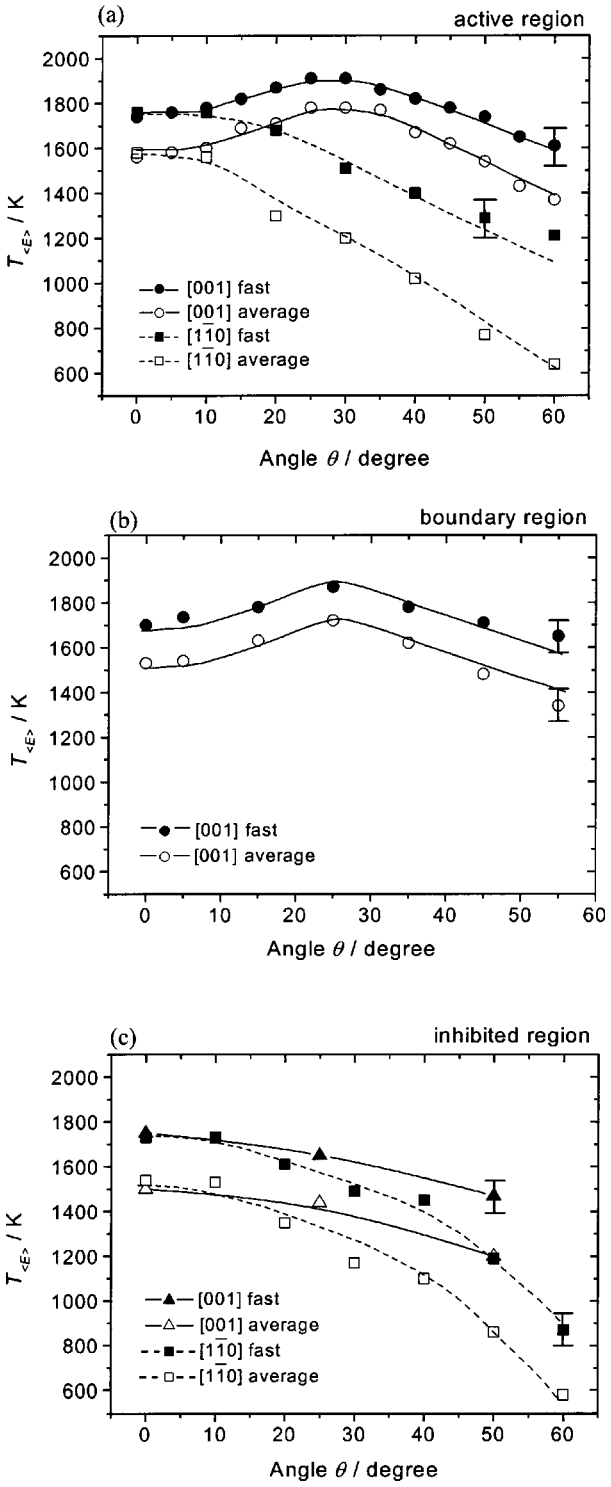

FIG. 11. The translational temperature vs the desorption angle at different crystal azimuths. (a) The active region, (b) the boundary region, and (c) the highly inhibited region. The average value calculated over all molecules before deconvolution of the velocity curve. The value for the fast component was estimated after deconvolution. The vertical bars indicate typical experimental errors.

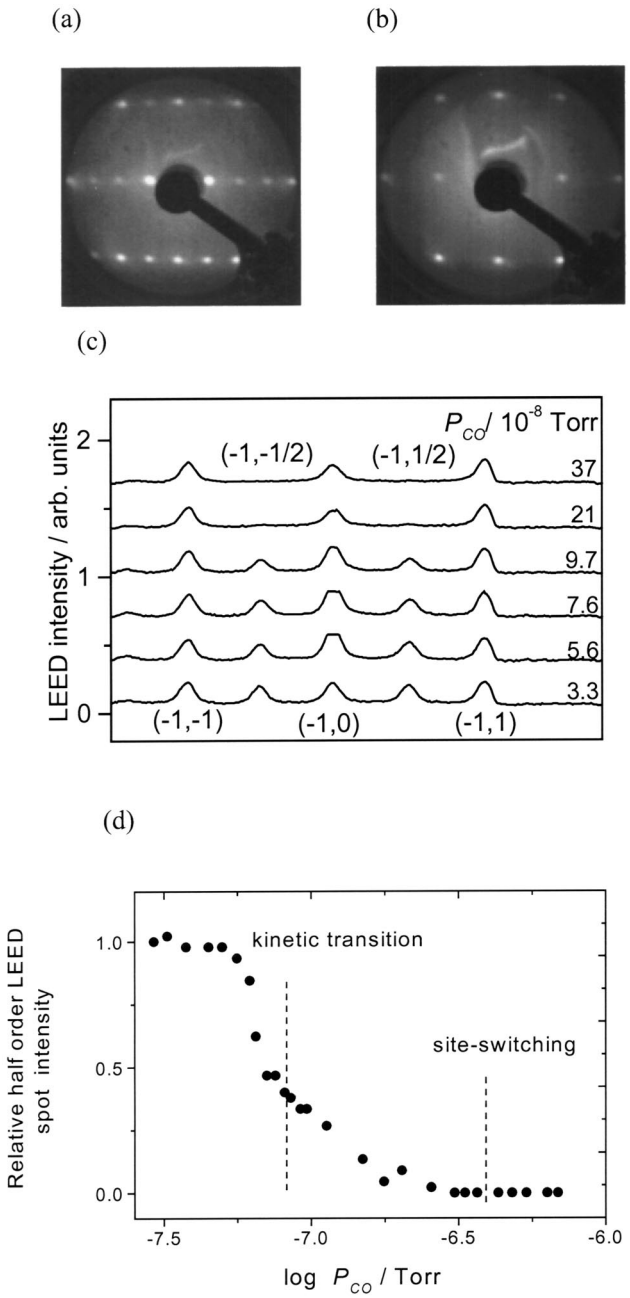

FIG. 12. LEED observations. Diffraction patterns recorded at the accelerated voltage of 78 eV (a) in the active region, and (b) above the site-switching. (c) LEED intensity profiles along the [001] direction at various P_{CO} values at fixed P_{O2} of 1×10^{-7} Torr and $T_S=490$ K. (d) Half-order LEED spot intensity against P_{CO}.

mally directed component is difficult because the pure component cannot be observed. The apparent distribution was approximated as a $\cos^3\theta$ form; however, it is inconsistent with the observed high velocity.

In the plane along the [110] direction, the distribution in the active region was deconvoluted into two components, i.e., one as sharp as $\cos^9\theta$ and the other one, a cosine component with the translational temperature equal to the surface temperature. The latter component was insignificant even at this azimuth. In the highly inhibited region, the distribution became broader and was approximated as $\cos^6\theta$ (Fig. 9).

On the (1×1) form, CO_2 desorption may collimate along the surface normal, as observed on Ir(110)(1×1).[21] The normally directed component obtained near or above the site-switching may be assigned to the formation on the (1×1) form. However, the normally directed component observed

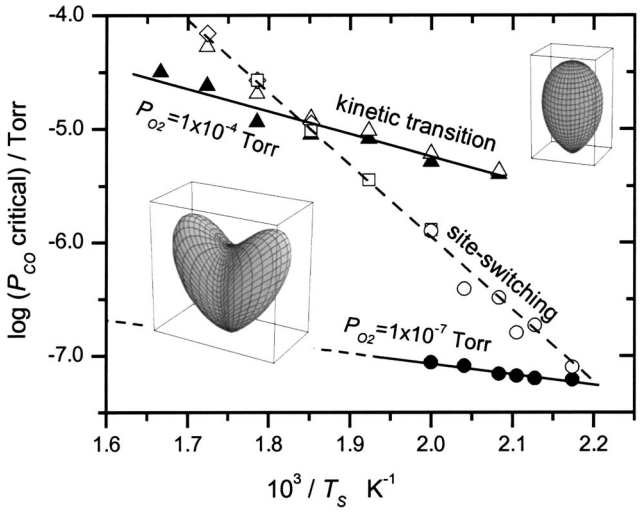

FIG. 13. Surface phase diagram. Logarithms of P_{CO} at the kinetic transition (closed symbols) and site-switching (open symbols) are plotted against the reciprocal of T_S and three-dimensional (3D) graphs representing spatial distribution in each region.

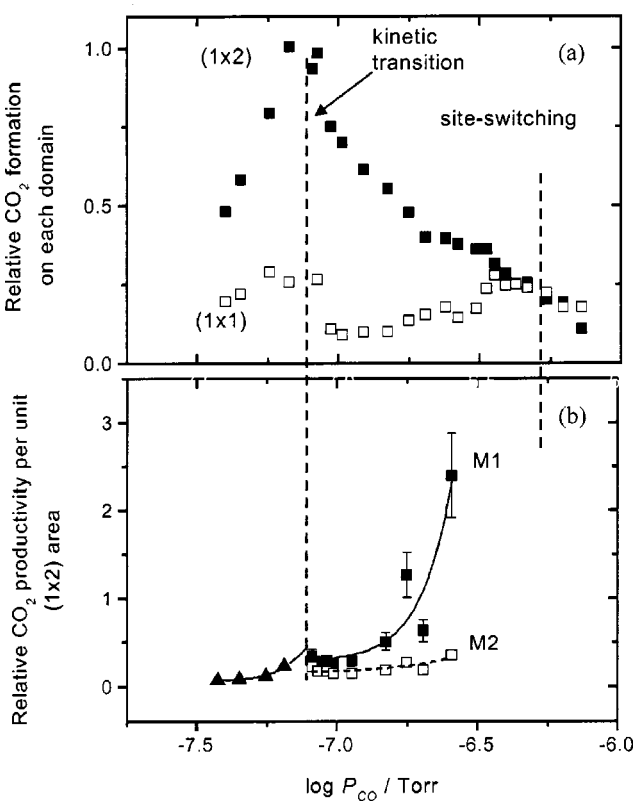

FIG. 14. Variation of the amount of CO_2 in the inclined desorption (■) and the normally directed one (□), with P_{CO} under steady-state reaction conditions. T_S was 490 K, and P_{O2} was 1×10^{-7} Torr. (b) The CO_2 productivity on (1×2) domains is the ratio of the total inclined desorption to the (1×2) domain area. The area was estimated from the half-order LEED spot intensity as (■): The linear dependence (M1), (□) the root square dependence (M2), (▲): The linear dependence-active region (see the text).

in the active region,[13] which was enhanced at lower CO pressure, cannot be assigned to the (1×1) form because Pt(110)(1×2) is stable in the presence of adsorbed oxygen. Recently, it has been shown that the normally directed CO_2 reactive desorption takes place even on the missing-row reconstructed surface when the surface is highly covered by oxygen, as exemplified on Rh(110) and Pd(110).[13,22] The enhanced normally directed desorption at low CO pressures is due to this mechanism and not due to the transformation into the (1×1) form.

B. CO_2 formation on (1×2)

CO(a) has a longer surface-residence time on oxygen-covered surfaces until its removal as CO_2 compared with its lifetime on one adsorption site[23] and can quickly and widely move over oxygen-covered areas at elevated temperatures. In fact, it has been satisfactorily confirmed theoretically[24] and experimentally[4] that CO is oxidized on sites for oxygen adsorption. Hence, the CO_2 formation is likely to proceed in oxygen-covered areas where the surface has a missing-row (1×2) structure.

The observed inclined CO_2 desorption is characteristic of the (1×2) domains because it is collimated along the normal direction of declining terraces on the (1×2) form with an excess translational energy. This component is major even when the share of (1×2) domains decreases rapidly, from around the kinetic transition towards the site-switching point. The normally directed component is produced on the (1×1) form, which must be stabilized by CO(a). We can simultaneously examine the productivity of CO_2 on both domains by analyzing the angular distributions and half-order spot LEED intensity. The total amounts of CO_2 in the deconvoluted components are shown for the boundary region in Fig. 14(a). The sharpness of the angular distribution of each component was considered in the calculation.[6] The CO_2 formation proceeds mostly on the (1×2) domains, and the contribution from the normally directed component is always minor, except for above the site-switching or far below the kinetic transition point.

Figure 12(d) shows the half-order spot intensity plotted against CO pressure. It is interesting to see the significant CO_2 desorption from (1×2) domains above the kinetic transition point and almost the disappearance of the half-order spot intensity. Figure 14(b) shows the CO_2 productivity per unit (1×2) area. This is the ratio of the total CO_2 formation from (1×2) domains to the half-order spot intensity, assuming that the intensity is proportional to the area of the (1×2) domain. The ratio increases in the active region about 5 times, i.e., more than the increment of the CO pressure. It increased steeply in the region between the kinetic transition and the site-switching point.

In general, the LEED intensity increases as the power of 1 to 2 with respect to the number of the unit lattice.[19] Here, we used the power of the first order in which the intensity was proportional to the number of the unit lattice (area) because the spot width did not become broad during measurements, and, furthermore, the (1×2) domain observed by PEEM was very large near the kinetic transition.[11] However, the power may increase depending on the distribution of the size of the (1×2) domains. Thus, in the figure, we also added the results of the case in which the second power describing the small size of the domain was used. Almost no difference

was found in the active region, whereas, in the boundary region, the ratio increment was suppressed to about a half of that in the former case, although it still increased.

C. Turnover frequency on (1×2)

The ratio of the product formation to the number of reaction sites is frequently used as the turnover frequency to present how many catalytic cycles proceed on one reaction site per unit time. On the present (1×2) domains, the area decreased more quickly than the decrease of CO_2 formation with increasing CO pressure in both the active and boundary regions. This does not necessarily mean the enhanced reactivity of the (1×2) domain. Rather, it shows that (1×2) domains have a high potential to produce CO_2. Usually, observation of this high potential is obscured in the overall reaction rate measurements because the CO_2 formation process has never been the rate-determining step under steady-state CO oxidation conditions on platinum metals.[1,23] In fact, the rate-determining step is either CO adsorption or O_2 dissociation.

In the active region, the supply of CO(a) to the (1×2) domains controls the CO_2 formation. This CO adsorption or diffusion rate increases with CO pressure in the active region, and the (1×2) domain decreases definitely. Thus, the apparent turnover frequency is enhanced in the active region. On the other hand, in the boundary region, the total CO_2 formation rate is controlled by O_2 dissociation because of the condition above the kinetic transition.[16] However, the surface oxygen is not quickly consumed since it is still covered by separate domains of (1×1) and (1×2) forms. The (1×1) domain is highly covered by CO(a) where the oxygen dissociation is slow. On the (1×2) domains, both the CO(a) and O(a) coverage must be small because the accumulation of CO(a) would convert the surface into the (1×1) form and O_2 dissociation is rate-determining. CO(a) can be easily supplied to the (1×2) domains from the (1×1) area. CO_2 can be formed on the (1×2) domains as long as O(a) is supplied from the surrounding (1×1) and domain boundaries as well as the (1×2) domain itself. The CO_2 formation in this region is controlled by these O(a) supplies. It deceases with increasing CO pressure, especially close to the site-switching point. Again, the CO_2 formation process itself is not rate-determining. The (1×2) domain decreases more quickly than the suppression of the O(a) supply, yielding the enhanced apparent turnover frequency. It should be noticed that the CO_2 formation on the (1×1) does not increase steeply in the boundary region [Fig. 14(a)]. The site preference to the (1×1) does not gradually shift over the boundary region. It takes place quickly close to the site-switching point.

D. CO_2 formation on (1×1)

The (1×1) structure under steady-state reaction conditions (above 450 K) can appear only when the surface is covered by CO, since the conversion from (1×1) to (1×2) takes place above 275 K. The total coverage required to convert into the (1×1) is 0.2 monolayer, and that to complete the conversion is 0.5 monolayer.[7] This means that, above the site-switching point, the surface is mostly covered by CO(a), close to 0.5 monolayer, except for a limited number of remaining (1×2) domains. Oxygen dissociation hardly takes place on the (1×1) plane stabilized by CO(a). Above the site-switching, CO_2 formation proceeds on oxygen dissociation sites immediately after dissociation, i.e., CO_2 production is suppressed unless O(a) is supplied from surrounding areas or after it is evacuated and O_2 is dissociated. These sites may be on (1×1) domains, ill-defined areas, for example, between domains, or structure defects.

The CO_2 desorption can be collimated along the surface normal at high coverage even when the surface is messy, as has been reported on polycrystalline surfaces.[25] Above the site-switching, it is difficult to determine separately the parameters of these desorption components from different sites. At present, the observed desorption was simply deconvoluted into two components by considering the observed velocity distributions, i.e., the normally directed desorption, which was temporally assigned to the formation on the (1×1) domains, and a cosine component. The latter was evaluated from the slow component in the velocity distributions.

E. CO_2 formation on domains border

Wintterlin *et al.* observed STM images of densely reactant-covered Pt(111) where CO(a) domains closely contacted with O(a) domains. CO_2 was proposed to be formed from O(a) and CO(a) between (2×2)-O and c(4×2)-CO domains.[26,27] This does not necessarily mean that CO_2 is always formed between closely contacted domains. The observed activation energy of about 11 kcal/mol is obtained only at very high reactant coverage. Furthermore, recent fast XPS observations of the oxygen signal indicated the presence of two kinds of reactive oxygen adatoms on this surface,[28] i.e., one showing the same reactivity as oxygen between contacted domains, and another showing around 20 times more reactivity than the former. This species appeared at coverages slightly less than those inducing closely contacted domains. This can be observed as streak images in scanning tunneling microscopy (STM). This species appears to be a more appropriate candidate of reactive oxygen under steady-state conditions.

It is well known that the reactive CO_2 desorption on Pt(111) collimates sharply along the surface normal direction over a wide coverage range.[25] The distribution is always collimated along the surface normal in a $\cos^{12-16}\theta$ form. The inclined desorption is not induced by the reaction site existing between domains. Furthermore, the CO_2 formation between domains has already been proposed on Pd(111) and Pd(100),[29,30] where the resultant desorption was collimated along the surface normal direction and the distribution became sharper at higher coverage.

F. Surface phase diagram

At the kinetic transition, CO adsorption balances with the removal of CO(a) as CO_2(g) and CO(g). The CO adsorption rate is insensitive to the surface temperature, i.e., no activation energy is required. On the other hand, the CO(a) removal process is sensitive to the surface temperature be-

cause both CO oxidation and CO desorption need significant activation energy. The activation energy of the former process has been estimated to be around 24 kcal/mol at low reactant coverage, and, at higher coverage, it has been estimated to decrease to about 11 kcal/mol.[23] On the other hand, the heat of CO adsorption, which should be equal to the activation energy for CO desorption, is 38 kcal/mol at low CO coverage and 33 kcal/mol at half a monolayer.[7] The kinetic transition shifted to higher CO pressures at higher O_2 pressures or at higher surface temperatures, yielding different activation energies. The value of 4.5–10 kcal/mol was actually obtained from the temperature dependence of the critical CO pressure at the kinetic transition. This value is too small compared with the above values, i.e., the temperature effect was somewhat compensated by other factors. Probably, the reactant density at the kinetic transition increases with decreasing the surface temperature.

The site-switching can be experimentally determined only by angular distribution measurements. This high sensitivity is due to the high potential of (1×2) domains to produce CO_2, i.e., CO_2 is mostly produced on this domain even when the domain is reduced to a nonvisible level by LEED. The critical CO pressure for the site-switching must be the threshold value to reach closely the half monolayer required for the complete surface transformation to the (1×1) form.[7] In other words, the site-switching line must be described by the CO adsorption isotherm at half a monolayer, i.e., it depends on P_{CO} and T_S values, and not on P_{O2} values. In fact, the observed activation energy derived from the slope in Fig. 13 yielded 31 kcal/mol, which is close to the heat of CO adsorption at half a monolayer. It always appears above the kinetic transition because of the necessity of the CO(a) accumulation to half a monolayer, and it is observed above the kinetic transition only when the amount of CO(a) is still below half a monolayer. When the CO coverage already exceeds this level at the kinetic transition, the site-switching line coalesces with the kinetic transition. Actually, the CO coverage at the site-switching may be somewhat less than this value because a significant CO_2 formation is still observed.

On the other hand, the kinetic transition line moves to higher CO pressures with increasing the oxygen pressure. This is expected from the enhanced removal of adsorbed CO(a) as CO_2(g) at higher O_2 pressures. This means that the kinetic transition line reaches the site-switching line at high O_2 pressures and reduces the boundary region. The boundary region cannot appear when the CO coverage just above the kinetic transition exceeds the critical CO coverage for the site-switching. Thus, the boundary region becomes wider at lower P_{O2} and higher T_S but it cannot be induced at high CO pressures.

G. Desorption on different sites

The boundary region between the kinetic transition and the site-switching provides a suitable stage for examining product desorption dynamics on individual reaction sites with different structures. This is because differently oriented sites coexist in the course of the catalyzed reaction. The product desorption dynamics can be separately studied at the same time and be compared with each other under the same conditions.

On the present surface, the translational temperature of desorbing product CO_2 at $T_S=560$ K is 1900 ± 80 K on (111) facets on Pt(110)(1×2) and 1730 ± 40 K on Pt(110)(1×1). The latter may be contributed from desorption over boundaries between domains. Under AR-thermal desorption spectroscopy (TDS) conditions, the value of 1370 K was reported for CO_2 from (111) terraces of Pt(110)(1×2) at 250 K.[31] This is not inconsistent with the present results because the value on (111) facets was reported to increase with increasing the surface temperature, with a slope of 1.5–2.0.[32]

This kind of energy comparison has only been reported on Pt(113)(1×2)=[s]3(111)$\times$3(001), which consists of three-atom wide (111) and (001) facets oriented differently.[6] Under steady-state CO oxidation conditions at 3×10^{-5} Torr O_2 and $T_S=555$ K, the value was reported to be about 1800 K for CO_2 desorbing from (111) terraces, and about 2200 K for that on (001) facets. In AR-TDS conditions, a value of about 1300 K was reported at around $T_S=300$ K on (111) facets.[33] The significant difference is again due to the surface temperature effect. On the other hand, the value on (001) facets was about 1200 K, far from the result at 555 K, suggesting the site modification.[6]

V. CONCLUSIONS

The steady-state CO oxidation on Pt(110) was studied by using angle-resolved product desorption measurements, velocity measurements, and LEED techniques. The following results were obtained:

(1) CO_2 desorption splits into two inclined components collimating at $\pm25°$ in the plane along the [001] direction, confirming that CO_2 desorption takes place on the (111) declining terraces of the (1×2) form. On the other hand, at high CO pressure, it desorbs along the surface normal;
(2) the velocity of desorbing CO_2 in the active region was maximized at $\theta=25°$ in the [001] direction and reached around 1900 K, whereas, in the inhibited region above the site-switching, it was maximized at the normal direction;
(3) the formation of CO_2 per unit area of (1×2) domains increased in both the active and inhibited regions, i.e., high CO_2 production was still observed despite the reduction of (1×2) domains;
(4) the site-switching represents the point where the structural transformation from (1×2) to (1×1) is completed. The surface phase diagram under steady-state reaction conditions has been constructed by following the CO pressure required for the site-switching and the kinetic transition.

ACKNOWLEDGMENTS

I.R. and Md.G.M. are indebted to the Ministry of Education, Sports, and Culture of Japan for their scholarship. L.M.G. acknowledges the support that he received from the

above Ministry through the COE invitation program (2001). This work was partly supported by a 1996 COE special equipment program of the said Ministry.

[1] T. Engel and G. Ertl, Adv. Catal. **28**, 1 (1979).
[2] J. A. Barker and D. J. Auerbach, Surf. Sci. Rep. **4**, 1 (1985).
[3] L. S. Brown and S. L. Bernasek, J. Chem. Phys. **82**, 2110 (1985).
[4] T. Matsushima, Heterog. Chem. Rev. **2**, 51 (1995).
[5] J. Dicke, P. Erchisen, J. Wolff, and H. H. Rotermund, Surf. Sci. **462**, 90 (2000).
[6] G. Cao, Md. G. Moula, Y. Ohno, and T. Matsushima, J. Phys. Chem. B **103**, 3235 (1999).
[7] T. E. Jackman, J. A. Davies, D. P. Jackson, W. N. Unertl, and P. R. Norton, Surf. Sci. **120**, 389 (1982).
[8] E. C. Sowa, M. A. Van Hove, and D. L. Adams, Surf. Sci. **199**, 174 (1988).
[9] T. Matsushima, Y. Ohno, and J. Murakami, Surf. Sci. **287/288**, 192 (1993).
[10] T. Matsushima, Surf. Sci. **242**, 489 (1991).
[11] S. Nettesheim, A. von Oertzen, H. H. Rotermund, and G. Ertl, J. Chem. Phys. **98**, 9977 (1993).
[12] A. von Oertzen, A. S. Mikhailov, H. H. Rotermund, and G. Ertl, J. Phys. Chem. B **102**, 4966 (1998).
[13] Md. G. Moula, A. B. P. Mishra, I. Rzeźnicka, M. U. Kislyuk, S. Liu, Y. Ohno, and T. Matsushima, Chem. Phys. Lett. **341**, 225 (2001).
[14] M. Kobayashi and Y. Tuzi, J. Vac. Sci. Technol. **16**, 685 (1979).
[15] G. Comsa, R. David, and B. J. Schumacher, Rev. Sci. Instrum. **52**, 789 (1981).
[16] T. Matsushima, D. B. Almy, and J. M. White, Surf. Sci. **67**, 89 (1977).
[17] Y. Ohno, T. Matsushima, and H. Miki, Surf. Sci. **281**, 234 (1993). [Equation (1) in this literature includes a typographical error. Its corrected form is given in the text.]
[18] I. Kobal and T. Matsushima, Trends Chem. Phys. **7**, 169 (1999).
[19] M. W. Roberts and C. S. McKee, in *Chemistry of the Metal-Gas Interface* (Oxford University Press, New York, 1978).
[20] M. W. Finis and V. J. Heine, J. Phys. F: Met. Phys. **4**, L37 (1974).
[21] T. Matsushima, Y. Ohno, and K. Nagai, J. Chem. Phys. **94**, 704 (1991).
[22] I. Rzeźnicka and T. Matsushima, Chem. Phys. Lett. **377**, 279 (2003).
[23] T. Campbell, G. Ertl, H. Kuipers, and J. Segner, J. Chem. Phys. **73**, 5862 (1980).
[24] A. Alavi, P. Hu, T. Deutsch, P. L. Silvestrelli, and J. Hutter, Phys. Rev.Lett. **80**, 3650 (1998).
[25] T. Matsushima, Surf. Sci. **127**, 403 (1983).
[26] T. Gritsch, D. Coulman, R. J. Behm, and G. Ertl, Appl. Phys. A: Solids Surf. **49**, 403 (1989).
[27] J. Wintterlin, S. Völkening, T. V. W. Janssens, T. Zambelli, and G. Ertl, Science **278**, 1931 (1997).
[28] I. Nakai, H. Kondoh, K. Amemiya, A. Nambu, T. Shimada, M. Nagasaka, and T. Ohta, in *Photon Factory Activity Report 2001* (High Energy Accelerator Research Organization, Tsukuba, 2002), p. 54.
[29] T. Matsushima and H. Asada, J. Chem. Phys. **85**, 1658 (1986).
[30] Y. Ohno, T. Matsushima, K. Shobatake, and H. Nozoye, Surf. Sci. **273**, 291 (1992).
[31] Y. Ohno, T. Matsushima, and H. Uetsuka, J. Chem. Phys. **101**, 5319 (1994).
[32] G. Cao, Y. Seimiya, and T. Matsushima, J. Mol. Catal. **141**, 63 (1999).
[33] P. K. Stefanov, Y. Ohno, T. Yamanaka, Y. Seimiya, K. Kimura, and T. Matsushima, Surf. Sci. **416**, 305 (1998).